SCIENTIFIC REPORTS

OPEN

Remote control of magnetostriction-based nanocontacts at room temperature

Received: 21 April 2015
Accepted: 31 July 2015
Published: 01 September 2015

S. Narayana Jammalamadaka[1], Sebastian Kuntz[2], Oliver Berg[2], Wolfram Kittler[2], U. Mohanan Kannan[1], J. Arout Chelvane[3] & Christoph Sürgers[2]

The remote control of the electrical conductance through nanosized junctions at room temperature will play an important role in future nano-electromechanical systems and electronic devices. This can be achieved by exploiting the magnetostriction effects of ferromagnetic materials. Here we report on the electrical conductance of magnetic nanocontacts obtained from wires of the giant magnetostrictive compound $Tb_{0.3}Dy_{0.7}Fe_{1.95}$ as an active element in a mechanically controlled break-junction device. The nanocontacts are reproducibly switched at room temperature between "open" (zero conductance) and "closed" (nonzero conductance) states by variation of a magnetic field applied perpendicularly to the long wire axis. Conductance measurements in a magnetic field oriented parallel to the long wire axis exhibit a different behaviour where the conductance switches between both states only in a limited field range close to the coercive field. Investigating the conductance in the regime of electron tunneling by mechanical or magnetostrictive control of the electrode separation enables an estimation of the magnetostriction. The present results pave the way to utilize the material in devices based on nano-electromechanical systems operating at room temperature.

The ability to manipulate and remotely control the electronic transport through single-atom or few-atom contacts is currently of great interest due to their potential applications in electronic devices[1] and nano-electromechanical systems (NEMS)[2]. In particular, mechanically-controlled break junctions[3,4], scanning tunneling microscopy[5], and electrochemical methods[6] have extensively been used to investigate the electronic transport through monatomic contacts. A mechanically-controlled break junction (MCBJ) is an electronic device where the distance between two metal electrodes can be tuned by bending the substrate to establish a contact comprising only a few or a single atom[3,4]. Several groups have reported interesting results on magnetic nano-contacts such as low-temperature magnetoresistance in ferromagnetic break junctions[7,8], conductance quantization in nickel (Ni) nanowires[9], tuning of magnetoresistance in nano-contacts by magnetostriction[10], and magnetoresistance of a single nickel atom[11]. Controlling the electrical conductance G in the range of a few G_0, where $G_0 = 2e^2/h = (12910\ \mathrm{Ohm})^{-1}$ is the conductance quantum, by an applied magnetic field H rather by mechanical control has been demonstrated recently by exploiting the large magnetostriction of the rare-earth element dysprosium at low temperatures[12].

Magnetostriction is a property of a ferromagnetic material that changes the volume of the material due to magnetic order. The magnetostrictive strain – the relative length change $\lambda = \Delta l/l$ in the direction of the magnetization – is associated with the magnetization process and depends on the applied magnetic field[13–19]. Typical values for the ferromagnets Fe, Co, and Ni are in the range of a few 10^{-6} at room temperature. Extensive work has been carried out to find a compound which exhibits a giant magnetostriction

[1]Magnetic Materials and Device Physics Laboratory, Department of Physics, Indian Institute of Technology Hyderabad, Hyderabad 502 205, India. [2]Physikalisches Institut, Karlsruhe Institute of Technology, Wolfgang Gaede Str. 1, Karlsruhe, 76131, Germany. [3]Defence Metallurgical Research Laboratory, Hyderabad 500058, India. Correspondence and requests for materials should be addressed to S.N.J. (email: surya@iith.ac.in) or C.S. (email:christoph.suergers@kit.edu)

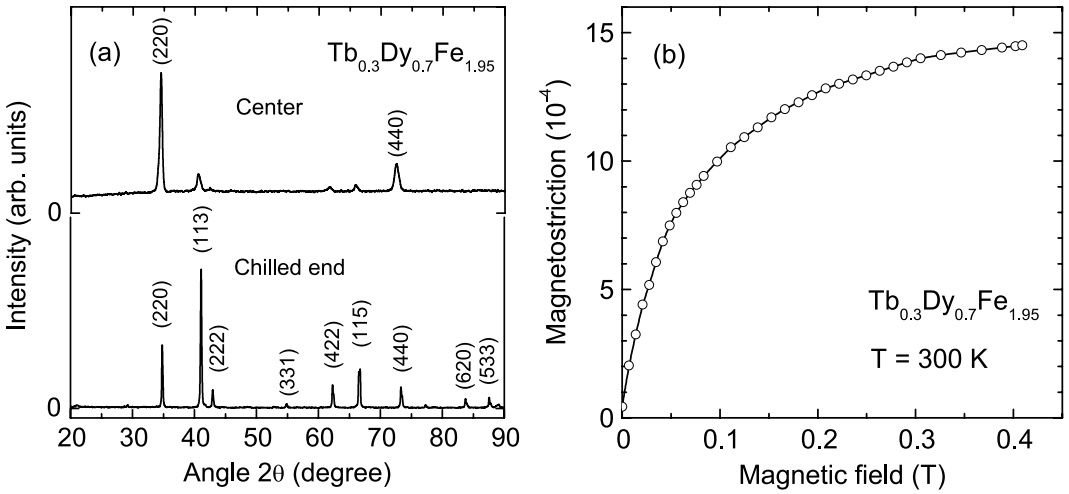

Figure 1. Texture and magnetostriction of $Tb_{0.3}Dy_{0.7}Fe_{1.95}$. (a) X-ray diffraction pattern (Cu K_α radiation) recorded with scattering vector oriented along the long axis of the rod. The data obtained at the chilled end (bottom) show a polycrystalline structure while the center part 5 cm away from the chilled end, which was slowly removed from the hot zone (top), has a strong fiber texture along the ⟨110⟩ direction. **(b)** Magnetostriction at room temperature measured with a strain gauge vs. magnetic field oriented along the long axis of the rod.

with low anisotropy at room temperature[13–19]. Among these compounds, the rare-earth transition-metal compound $(Tb_{0.27}Dy_{0.73})Fe_{1.95}$ with cubic structure is commercially available as rods under the name Terfenol-D[18]. The material properties can be further tuned to obtain the anisotropy-compensated compound $Tb_{0.3}Dy_{0.7}Fe_{1.95}$ with low first-order magnetocrystalline anisotropy constant $K_1 = -6 \times 10^4 Jm^{-3}$ and huge magnetostriction $\lambda = 1.6 \times 10^{-3}$ at room temperature[20]. This material can be used in the form of wires to realize a magnetic-field operated "nanoswitch" at room temperature. However, the machining of this material is extremely difficult as its Young's modulus is extremely low[16,17].

Conductance measurements have been reported for single-element based atomic junctions but not for junctions comprising multi-element compounds[21,22], in particular not for devices exploiting giant-magnetostriction phenomena at room temperature. Since $Tb_{0.3}Dy_{0.7}Fe_{1.95}$ has a giant magnetostrictive strain at room temperature, the gap between single atoms or few atoms could be controlled in a remote way without mechanical access, which would be beneficial compared to conventional MCBJ devices. In the present work, we have realized the aforementioned ideas on $Tb_{0.3}Dy_{0.7}Fe_{1.95}$ based nano-contact devices. The contacts can be switched at room temperature by a magnetic field and the observed behaviour is in qualitative agreement with the magnetization process. The conductance switching strongly depends on the field orientation with respect to the contact due to the magnetic anisotropy. Comparison of the electron tunneling data when controlling the gap between two contacts either mechanically or by magnetic field allows an estimation of the magnetostriction of $Tb_{0.3}Dy_{0.7}Fe_{1.95}$.

Results

Characterization of $Tb_{0.3}Dy_{0.7}Fe_{1.95}$. A $Tb_{0.3}Dy_{0.7}Fe_{1.95}$ rod was obtained by employing a modified Bridgman method for crystal growth, see Methods section. Figure 1(a) shows the x-ray diffraction (XRD) pattern of two pieces of material. The data obtained from a piece cut from the chilled end of the rod (bottom) indicate a polycristalline structure, while the piece cut from the part slowly retracted from the hot zone 5 cm from the chilled end (top) has a preferred orientation with the crystallographic ⟨110⟩ axes along the rod axis. The ⟨110⟩ direction makes an angle of 35 degrees with the ⟨111⟩ direction which is the magnetic easy-axis[16,18–20]. Pieces cut from this directionally solidified part of the rod were used for the conductance and magnetostriction measurements. The magnetostriction vs. magnetic field H is plotted in Fig. 1(b) which confirms a giant value of $\lambda \approx 1.5 \times 10^{-3}$ in 0.4 Tesla at room temperature.

The MCBJ device. Figure 2(a) shows a schematic of the MCBJ device. The material under study (grey) is fixed to a flexible substrate which can be bended mechanically by pushing a piston against the back of the substrate. Fine tuning of the bending is achieved by using a voltage controlled piezo stack[12]. In the present case, $Tb_{0.3}Dy_{0.7}Fe_{1.95}$ thin wires of $\approx 1 \times 1\,mm^2$ cross section and 8 mm length were obtained by carefully shaping appropriate pieces with emery paper and subsequent cleaning by ultrasonic vibration. Copper wires were connected to the sample by conductive silver epoxy Epo-Tek H20E to perform four-point conductance measurements. The sample with attached Cu wires was almost completely covered with Stycast 2850FT epoxy and glued to a flexible ($5.5 \times 10.5\,mm^2$), 0.3 mm thick copper-bronze

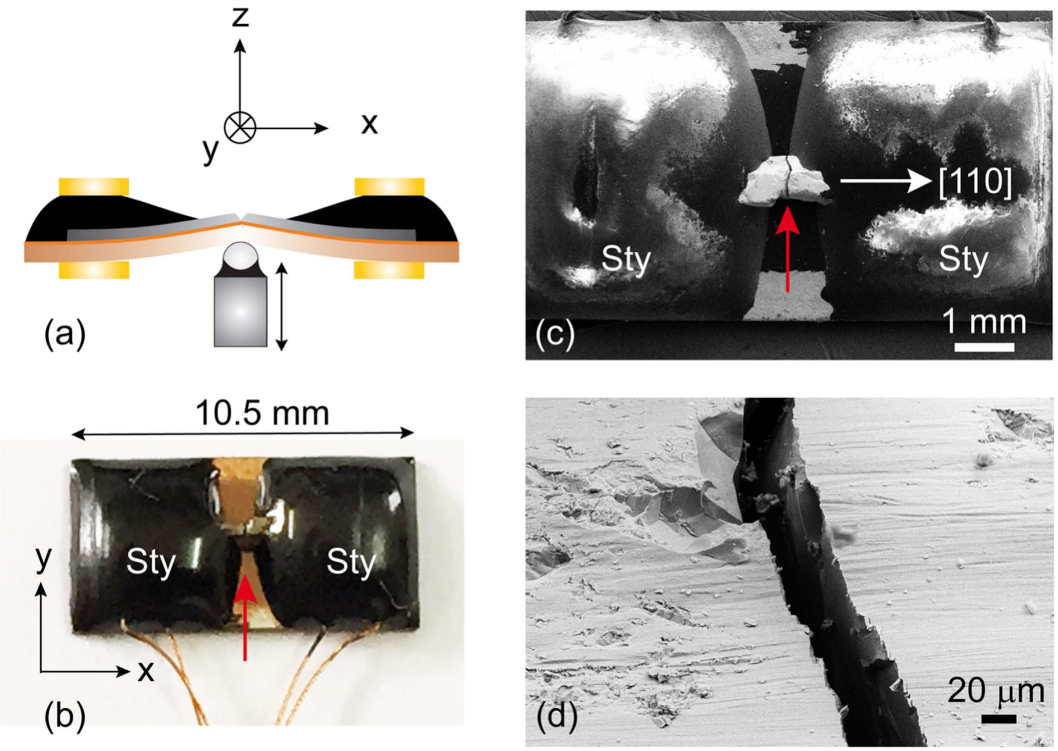

Figure 2. Mechanically-controlled break junction of $Tb_{0.3}Dy_{0.7}Fe_{1.95}$. (a) Schematic (side view) of the $Tb_{0.3}Dy_{0.7}Fe_{1.95}$ wire (grey) glued with Stycast epoxy (black) to the Cu bronze substrate (brown) fixed between metallic supports (yellow). The substrate can be bended by pushing the piezo-driven rod from below. **(b)** Photograph (top view) of a 8-mm long $Tb_{0.3}Dy_{0.7}Fe_{1.95}$ sample with Cu wires attached. The sample and the electrical contacts are almost completely covered by Stycast epoxy (Sty) apart from the inner 2 mm where the material breaks (red arrow) and forms a junction. **(c)** SEM image of the ⟨110⟩-oriented wire (top view). Red arrow indicates the junction, Sty indicates the Stycast epoxy drops. **(d)** SEM image of the junction seen under an oblique angle. The SEM images show a clear rupture of the order of 20 μm at the junction between the electrodes due to mechanical breaking.

substrate coated with a 2 μm thick durimide film for electrical insulation, see Fig. 2(b,c). A notch was created in the inner region ($\approx$ 2 mm) not covered by Stycast epoxy in order to predefine the position where the wire breaks during bending the substrate. The magnetic field was oriented along the z direction in measurements at room temperature or along the x or y direction in measurements at $T = 4.2$ K.

Switching the contact at room temperature. Figure 3(a) shows the electrical conductance G vs. magnetic field H for a grain oriented $Tb_{0.3}Dy_{0.7}Fe_{1.95}$ break junction at room temperature with the magnetic field applied in the z direction. Initially, the junction was adjusted to be in weak contact at $G \approx 100$–$1000\ G_0$ by mechanically bending the substrate. This conductance corresponds to a junction with a contact diameter of a few nm[3]. After a few cycles of initial switching without hysteresis the contact reproducibly switches from a "closed" ($G > 0$) to an "open" ($G = 0$) state when the magnetic field increases from zero to above 0.5 T. The finite conductance of $\approx 10^{-2} G/G_0$ measured in the open state is due to the 1 MΩ resistor connected in parallel to the device, see Methods section. The arrows in the graph indicate the evolution of the conductance during the field sweep. The device configuration at each state is visualized by cartoons (brown colour). This switching behaviour of the conductance was measured several times and was established on several samples. The field dependence of the magnetization M in a magnetic field H_z oriented perpendicularly to the long wire axis shows a hard-axis behaviour, see Fig. 3(b).

From $M(H_z)$ the qualitative behaviour of the magnetostrictive strains λ_z and λ_x in the z and x direction, respectively, are obtained. Usually, the uniaxial magnetostrictive strain along a hard axis is roughly proportional to the square of M, i.e., $\lambda/\lambda_s = M^2/M_s^2$, where M_s and $\lambda_s > 0$ are the saturation values measured in a high magnetic field of 2 T[17]. The field dependence of λ_z is shown in Fig. 3(c) (solid line). However, the conductance of the device depends only on the electrode separation along the x direction which is affected by magnetostriction. For polycrystals, the magnetostriction in the x direction perpendicular to the magnetization is approximated by $\lambda_x/\lambda_{xs} = -\lambda_z/2\lambda_{zs}$ shown in Fig. 3(c) (dashed line)[17]. Hence, starting from a closed contact in zero field the electrodes should increase in diameter along the

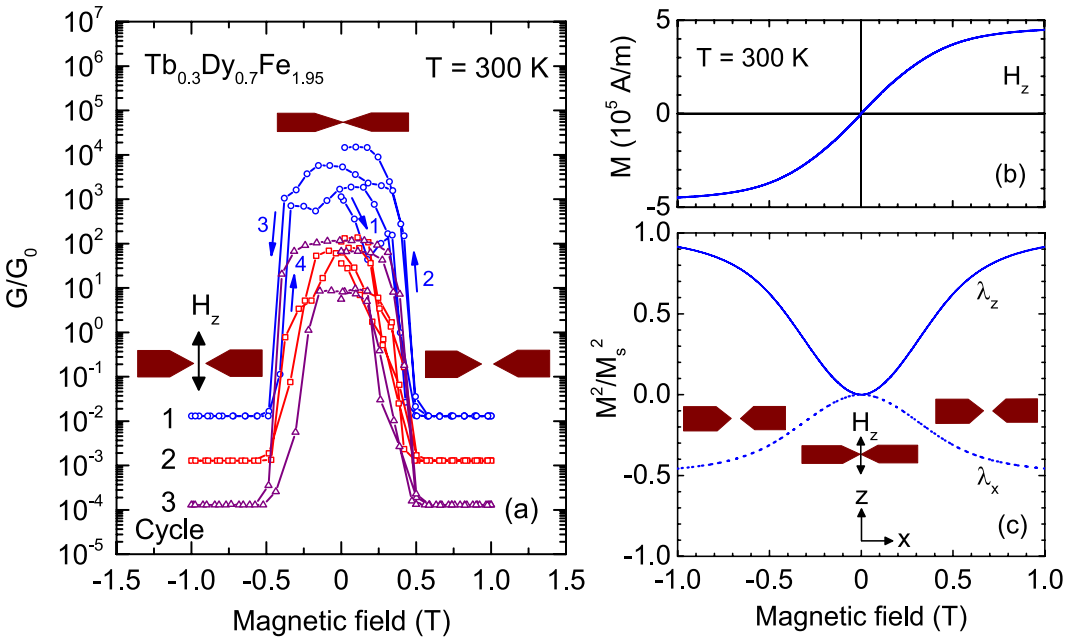

Figure 3. Magnetostriction-controlled conductance switching of $Tb_{0.3}Dy_{0.7}Fe_{1.95}$ at room temperature. **(a)** Semi-logarithmic plot of the conductance G in a magnetic field H_z applied along the z axis. Cycles 2 and 3 have been successively shifted downward by one decade with respect to cycle 1 for clarity. Cartoons visualize the contact configuration in magnetic field due to magnetostriction. **(b)** Magnetization M vs. H_z. **(c)** M^2/M_s^2 calculated from $M(H_z)$ (solid line) shows the qualitative behaviour of the magnetostrictive strain λ_z in H_z. The corresponding strain along the wire axis (dashed line) is approximated by $\lambda_x = -\lambda_z/2$.

z direction and shrink their length along the x direction with increasing field due to the positive magnetostriction of the material. This leads to an opening of the contact in high magnetic fields as observed in Fig. 3(a).

Switching the contact at different temperatures. The effect of temperature on the switching of the conductance $G(H)$ was investigated in the temperature range 10–300 K. Figure 4(a–d) shows exemplary $G(H)$ curves of the $Tb_{0.3}Dy_{0.7}Fe_{1.95}$ break junction at various temperatures. We observe a switching between high conductance and low conductance at each temperature. In these measurements, the contact was initially adjusted in an "open" state in high magnetic field and then the field was reduced. Hence, the maximum of G depends on the arbitrary electrode separation before performing the field sweep. The difference in the maxima between up and down sweeps is attributed to changes of the nanocontact configuration when the contact opens and closes several times during performing a complete field loop.

At temperatures below 70 K we observe a hysteresis of the switching in $G(H)$ which is also seen in the magnetization curves $M(H)$ shown in Fig. 4(e–h). However, the maxima in $G(H)$ [Fig. 4(a,b)] occur at higher magnetic fields than the coercive fields in $M(H)$ [Fig. 4(e,f)]. This is presumably due to deviations of the local micromagnetic structure close to the nanocontact from the volume-integrated magnetization $M(H)$ measured by the magnetometer. Nevertheless, the qualitative behaviour between $G(H)$ and $M(H)$ is the same regarding the occurrence of a hysteresis below 70 K. The reason for the hysteresis might be a pinning of magnetic domain walls. In Ni-substituted $Dy_{0.73}Tb_{0.27}Fe_2$, a maximum in the temperature dependence of the magnetization in 1 T for $T < 50$ K was attributed to the strong pinning of domain walls at $T = 4.2$ K and the decrease of the pinning barrier with increasing temperature[23]. This suggests that a similar effect of domain wall pinning gives rise to the hysteresis in the magnetization and in the conductance switching of $Tb_{0.3}Dy_{0.7}Fe_{1.95}$ nanocontacts at temperatures below 70 K which disappears at higher temperatures.

We now focus on the conductance switching performed at constant temperature $T = 4.2$ K for different orientations of the magnetic field to explore the effect of magnetic anisotropy on the switching behaviour. The magnetic field could be rotated in the x-y plane of the sample either parallel (x) or perpendicular (y) to the long wire axis. In nanocontact devices, a hysteresis of $M(H)$ can cause negative magnetostrain, which would eventually alter the magnetostriction behaviour $\lambda(H)$[12]. To avoid such effects, we demagnetized the contact before we started the field sweep. Figure 5(a) shows a measurement performed at $T = 4.2$ K with the magnetic field H_y oriented perpendicularly to the long wire axis (y direction). In this configuration, the device was in the "closed" state before application of the magnetic field. With increasing field H_y the conductance drops at a magnetic field of 0.4–0.5 T and the contact opens due to the extension of the wire diameter along the field (y direction) and the corresponding shrinkage along

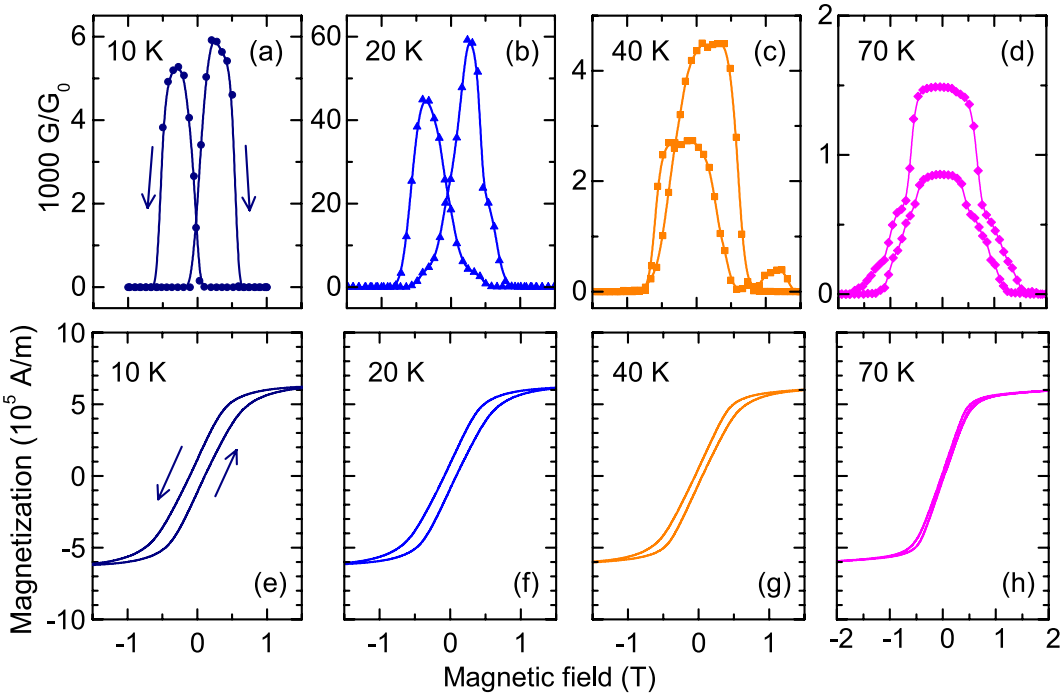

Figure 4. Temperature dependence of magnetostriction-controlled conductance switching of $Tb_{0.3}Dy_{0.7}Fe_{1.95}$. (a–d) Conductance vs. magnetic field applied perpendicularly to the long wire axis. **(e–h)** Magnetization curves in perpendicular magnetic field at various temperatures. A hysteresis loop opens below 70 K in accordance with the hysteresis observed in the conductance switching.

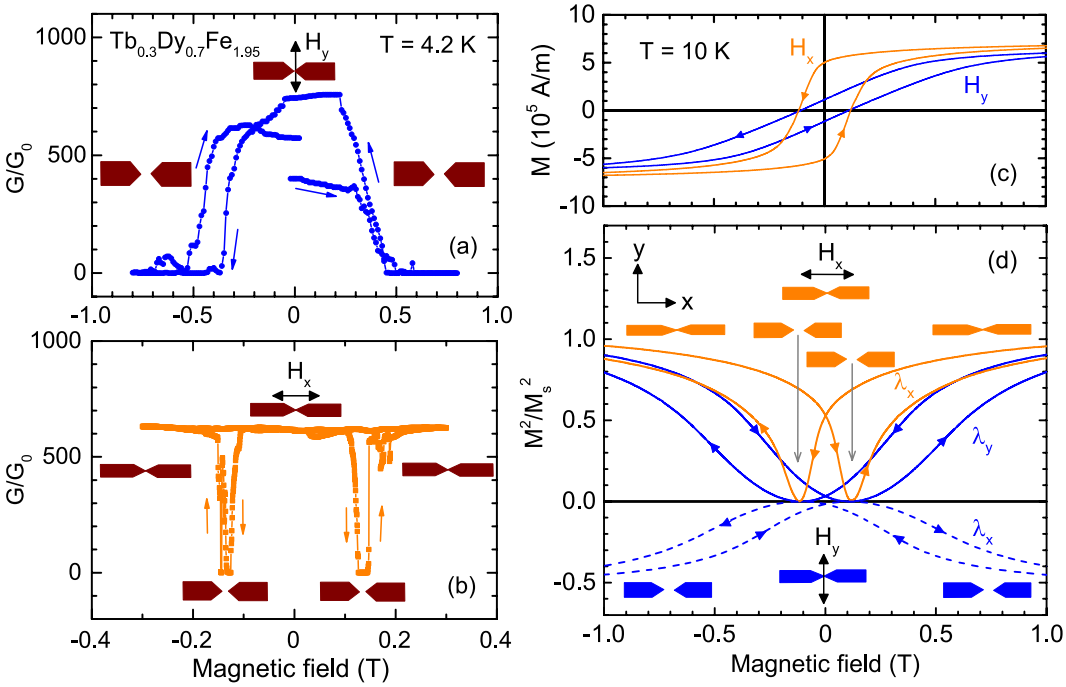

Figure 5. Conductance switching of $Tb_{0.3}Dy_{0.7}Fe_{1.95}$ at low temperatures in different field orientations. (a) Conductance G/G_0 in perpendicular field H_y at $T = 4.2$ K. **(b)** Conductance G/G_0 in parallel field H_x at $T = 4.2$ K. **(c)** Magnetization loops obtained at $T = 10$ K. **(d)** Qualitative behaviour of the magnetostrictive strains λ_x and λ_y calculated from M^2/M_s^2 in H_x and H_y (solid lines), see text for details. In perpendicular field H_y, the strain along the long wire axis is $\lambda_x = -\lambda_y/2$ (dashed line). Cartoons visualize the contact configuration in magnetic field due to magnetostriction.

the wire axis (x direction) due to magnetostriction. In addition, we observe a hysteresis in the switching at negative field due to a hysteresis in the magnetization curve shown in Fig. 5(c) with a coercivity $\mu_0 H_c = 0.12$ T. For this sample a corresponding hysteresis at positive fields is missing. One reason for this asymmetric behaviour might be the different magnetic domain configurations when the magnetic field is rotated by 180°. We calculate the field dependence of the magnetostrictive strain from the magnetization curve $M(H_y)$ of Fig. 5(c) in both directions as mentioned above, see Fig. 5(d) (blue curves). The behaviour of the magnetostrictive strain $\lambda_x(H_y)/\lambda_{xs}$ along the long wire axis x (dashed line) resembles the behaviour of $G(H_y)$. The smooth variation of the magnetostrain with increasing field towards negative values along the x direction gives rise to an increasing separation between the two electrodes until the contact opens. The closing of the contact around zero field is in agreement with the $M^2(H_y)$ behaviour, see Fig. 5(d) (dashed curve).

In a magnetic field H_x applied parallel to the long wire axis a different switching behaviour is observed, see Fig. 5(b). Starting from a "closed" state and increasing the field, the conductance is almost constant up to ≈0.1 T where G sharply drops to zero representing the opening of the contact. By increasing the field further to ≈0.15 T the conductance suddenly recovers and reaches its zero-field value at high fields indicating a closed contact. Reducing the field subsequently and sweeping to negative field values does not change the conductance until between −0.1 and −0.15 T the same behaviour is observed like for positive fields. The switching behaviour with two sharp dips of $G(H)$ at ≈ ±0.15 T is in qualitative agreement with the behaviour of the magnetization and corresponding magnetostrictive strain. Figure 5(c) shows the magnetization of the sample vs. field H_x representing a more rectangular hysteresis loop with a coercive field $\mu_0 H_c = 0.12$ T, similar to H_c obtained in perpendicular field H_y. The different shape of $M(H)$ in the two field orientations demonstrates the magnetic anisotropy of the ⟨110⟩-oriented sample. The almost rectangular loop gives rise to a strong field dependence of the magnetostrain derived from $M^2(H_x)/M_s^2$ plotted in Fig. 5(d) (yellow curve). In particular, the magnetostrain is almost zero close to the coercive field due to the reorientation of magnetic domains and $M = 0$ at H_c. However, above and below H_c, the magnetostrain is large due to the strong variation of $M(H_x)$ which gives rise to two dips in λ_x close to H_c. This field dependence immediately explains the observed switching of the nanocontact in parallel field H_x [Fig. 5(b)]. Starting at a closed state at zero field after magnetizing the sample, the magnetostrain along the x direction strongly drops close to H_c leading to an opening of the contact. After the reorientation of domains for fields $H_x > H_c$ the magnetostrain rises and the contact closes again. This is supported by the fact that the opening of the contact and the drop of conductance start to occur at H_c, cf. Fig. 5(b). Hence, the magnetic anisotropy of the material strongly affects the magnetostriction-controlled switching behaviour of the break junction in different orientations of the magnetic field.

Estimation of the magnetostriction from the tunneling conductance. Once the contact has been adjusted to exhibit a conductance well below G_0, the electronic transport is dominated by tunneling. The tunneling current depends on the gap between the two electrodes which can be controlled mechanically or by magnetostriction. The comparison of the tunneling behaviour observed in both cases allows an estimation of the magnetostriction as we demonstrate in the following. However, in the present case the tunneling behaviour could only be observed at low temperatures.

Figure 6 shows ln (G/G_0) vs. piezo voltage, i.e., electrode separation along the x direction, for $G/G_0 \ll 1$ at $T = 10$ K indicating an exponential decay of the conductance with electrode separation Δx characteristic for electron tunneling

$$G/G_0 = exp\left(\frac{-\Delta x}{\xi}\right) \tag{1}$$

where $\xi = h/4\pi\sqrt{2m^*\phi}$, h is the Planck constant, m^* is effective electron mass, and ϕ is the average electronic work function of $Tb_{0.3}Dy_{0.7}Fe_{1.95}$. An average work function $\phi = 5.9$ eV and $\xi = 0.4$ Å was used for $Tb_{0.3}Dy_{0.7}Fe_{1.95}$ by considering the individual work functions of the constituents and by taking into account the change of the work function in helium atmosphere[24]. From the linear slope $1/\xi_V$ of the semi-logarithmic plot of $G(V)$ in Fig. 6 and considering $\Delta x/\xi = \Delta V/\xi_V$ we estimate a variation of the gap by the piezo voltage to 2.0 Å/V.

A similar calculation can be performed when the gap is controlled by magnetostriction. Figure 6 shows $\ln(G/G_0)$ vs. perpendicular magnetic field at 10 K. Again, the $G(H)$ data measured during closing show an exponential behaviour characteristic for electron tunnneling with a slope $1/\xi_H$ in a $\ln(G/G_0)$ vs. H plot[12,25]. The variation of the electrode distance, i.e., the gap Δx, by a field variation around $\mu_0 H = 1$ T is calculated from $\Delta x/\xi = \mu_0 \Delta H/\xi_H$ similarly to the mechanical control above. We obtain $\Delta x/\mu_0 \Delta H = 5.3$ nm/T for the increase of the gap with increasing field, corresponding to a relative shrinkage of the wire length $\Delta L/L = -2.7 \times 10^{-6}$ along the x direction ($L \approx 2$ mm). The observed field-induced gap variation in x direction is caused by the magnetostrain due to the corresponding increase of the wire diameter by $-2\Delta L/L = 5.4 \times 10^{-6}$ along the magnetic field in perpendicular direction. From this we estimate the magnetostriction of $Tb_{0.3}Dy_{0.7}Fe_{1.95}$ at 10 K by

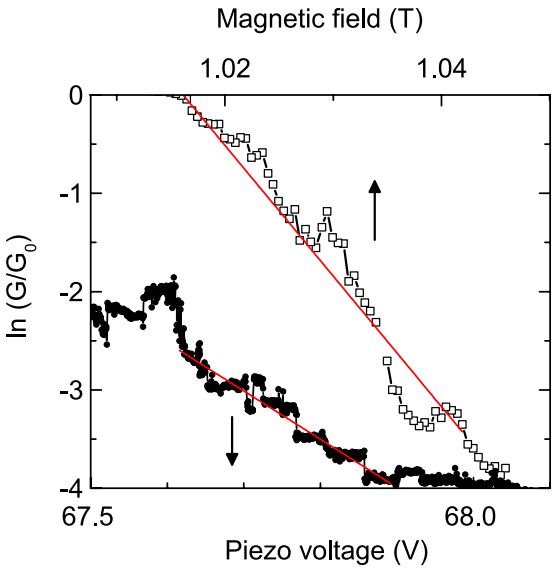

Figure 6. Conductance in the regime of electron tunneling. Semilogarithmic plot of G/G_0 vs. piezo voltage or magnetic field applied perpendicularly to the long wire axis at $T = 10$ K. Red lines indicate a linear dependence $\ln(G/G_0) \propto V$ or $\ln(G/G_0) \propto H$, respectively.

$$d\lambda/dH = \lambda_s \, d\,(M^2/M_s^2)/dH \tag{2}$$

Here, $d\,(M^2/M_s^2)/dH \approx 0.5/\mathrm{T}$ is the slope of M^2/M_s^2 representing λ in perpendicular field around $\mu_0 H = 1$ T [Fig. 5(d) blue curve]. Hence, we obtain a low saturation magnetostriction $\lambda_s \approx 1 \times 10^{-5}$ for $Tb_{0.3}Dy_{0.7}Fe_{1.95}$ at 10 K, two orders of magnitude smaller than at room temperature[26,27].

Discussion

The results clearly demonstrate the remote control of the nanocontact conductance by a magnetic field. We mention that the measurements for Dy nanocontacts reported earlier[12] were constrained to low temperatures, where Dy is in a ferromagnetic state and has a large magnetostriction. In the present case of $Tb_{0.3}Dy_{0.7}Fe_{1.95}$ the conductance of the wire switches at room temperature due the giant magnetostrictive property of this material. The magnetocrystalline and shape anisotropy of the wire plays an important role for the switching behaviour. Application of a magnetic field along the magnetic hard axis, i.e., perpendicular to the long wire axis, is beneficial because in this case the wire is strained continuously without hysteresis. In contrast, if the magnetic field is applied along the magnetic easy axis, i.e., along the long wire axis, an abrupt switching is obtained in a limited field range close to the coercive field where the magnetization spontaneously rotates by 180°. The hysteresis observed in the *G(H)* behaviour at low temperature is attributed to the temperature dependence of the magnetization curves and the pinning of the domain walls at low temperatures. Hence, the switching behaviour in parallel and perpendicular field is entirely different due to the different magnetic anisotropy in the two orientations. From the piezo-voltage as well as magnetic-field control of the conductance, we are able to estimate the field-induced length changes of the contact and the magnetostriction of $Tb_{0.3}Dy_{0.7}Fe_{1.95}$ at low temperatures. In conclusion, we have realized a magnetic-field induced switching of the conductance G of break junctions made from the giant magnetostrictive compound $Tb_{0.3}Dy_{0.7}Fe_{1.95}$ at room temperature. The results are important when developing future devices based on NEMS.

Methods

A $Tb_{0.3}Dy_{0.7}Fe_{1.95}$ compound was prepared in a vacuum induction-furnace by casting the liquid alloy into quartz tubes placed over a water-cooled copper plate. The cast rod was then directionally solidified employing a modified Bridgman technique under high vacuum (10^{-6} mbar). During the directional solidification process, the rod was fixed on a retractable water-cooled copper chilling plate which was then slowly retracted from the hot zone (1350° C) at a constant pulling rate of 70 cm/h. Accordingly, cylindrical directionally solidified rods of 10 cm length and 20 mm diameter were prepared. Since the portion which is in touch with the copper plate does not melt we have taken a sample from the center of the rod at a distance 5 cm from the chilled end for device fabrication. Material characterization was done by back-scattered electron microscopy of the directionally solidified compound along the longitudinal

direction and by energy dispersive spectroscopy confirming the presence of single phase with uniform composition along the entire sample.

The room-temperature magnetostriction of $Tb_{0.3}Dy_{0.7}Fe_{1.95}$ was determined on a separate sample cut from the center of the same rod. A commercially available temperature-compensated 120 Ohm Karma-foil strain gauge with low magnetoresistance (Micro-Measurements Group Inc., USA) was directly attached to the sample with Cynoacrylate cement (M-bond 200 or Anabond 202). The leads were soldered to fine copper wires (SWG 38) for resistance measurements with a Wheatstone bridge. The sample with the strain gauge was carefully placed in between the pole pieces of an electromagnet with the magnetic field applied parallel to the rod axis. The relative length change due to magnetostriction $\Delta l/l$ was calculated from $\Delta l/l = 4\Delta E/VK$, where ΔE is the unbalanced bridge voltage, V is the excitation voltage and K a the gauge calibration factor.

For the conductance measurements, a 1 MΩ resistor was connected in parallel to the MCBJ as a shunt to avoid large voltage spikes across the contact during opening or closing. The assembly was mounted in a MCBJ device, which was inserted into a physical property measurement system (PPMS, Quantum Design) providing a magnetic field in the z direction perpendicular to the substrate surface. Before breaking the wire, the sample chamber was purged many times with helium gas. In addition, a cryopump was connected to the sample chamber to achieve high-to-ultrahigh vacuum conditions. Mechanical instabilities were minimized by tightly fixing both ends of the wire to the nonmagnetic substrate with high-quality stycast. In addition, before collecting data the temperature of the MCBJ was stabilized to about 1 mK a long period of time.

For performing measurements in different field orientations, the MCBJ was inserted into the liquid ^{4}He bath ($T = 4.2$ K) of another cryostat equipped with a superconducting Helmholtz coil providing a magnetic field in the x-y plane of the substrate. The field orientation parallel (x direction) or perpendicular (y direction) to the long wire axis could be changed by rotating the MCBJ device around the substrate normal. The wire was mechanically broken by using a pushing rod which was driven by a stepper motor. Fine tuning of the electrode distance was achieved by a voltage-driven pizo stack between the pushing rod and the substrate. The conductance was monitored by measuring the voltage at a constant current of 1 μA.

The magnetization was measured in a vibrating-sample magnetometer (VSM, Oxford Instruments) at different temperatures between 10 K and 300 K for field orientations parallel or perpendicular to the long wire axis. The sample was vibrating at a frequency of 55 Hz with an amplitude of 0.2 mm. The magnetization was calculated from the measured magnetic moment by using a mass density of 9.25 gcm^{-3}.

Scanning electron-microscopy (SEM) images were recorded with various magnifications at a beam energy of 20 keV in a Carl Zeiss Supra 40 electron microscope.

References

1. Xiang, D. *et al.* Three-Terminal Single-Molecule Junctions Formed by Mechanically Controllable Break Junctions with Side Gating. *Nano Lett.* **13,** 2809–2813 (2013).
2. Tsutsui, M., Morikawa, T., Arima, A. & Taniguchi, M. Thermoelectricity in atom-sized junctions at room temperatures. *Sci. Rep.* **3,** 3326 (2013).
3. Agrait, N., Yeyati, A. L. & van Ruitenbeek, J. M. Quantum properties of atomic-sized conductors. *Phys. Rep.* **377,** 81–279 (2003).
4. Scheer, E. *et al.* The signature of chemical valence in the electrical conduction through a single-atom contact. *Nature* **394,** 154–157 (1998).
5. Brandbyge, M. *et al.* Quantized conductance in atom-sized wires between two metals. *Phys. Rev. B* **52,** 8499–8514 (1995).
6. Xie, F.-Q., Nittler, L., Obermair, C. & Schimmel, T. Gate-Controlled Atomic Quantum Switch. *Phys. Rev. Lett.* **93,** 128303 (2004).
7. Bolotin, K. I., Kuemmeth, F., Pasupathy, A. N. & Ralph, D. C. From Ballistic Transport to Tunneling in Electromigrated Ferromagnetic Breakjunctions. *Nano Lett.* **6,** 123–127 (2006).
8. Egle, S. *et al.* Magnetoresistance of atomic-size contacts realized with mechanically controllable break junctions. *Phys. Rev. B* **81,** 134402 (2010).
9. Ono, T., Ooka, Y., Miyajima, H. & Otani, Y. $2e^2/h$ to e^2/h switching of quantum conductance associated with a change in nanoscale ferromagnetic domain structure. *Appl. Phys. Lett.* **75,** 1622–1624 (1999).
10. Gabureac, M., Viret, M., Ott, F. & Fermon, C. Magnetoresistance in nanocontacts induced by magnetostrictive effects. *Phys. Rev. B* **69,** 100401 (2004).
11. Viret, M. *et al.* Magnetoresistance through a single nickel atom. *Phys. Rev. B* **66,** 220401 (2002).
12. Müller, M. *et al.* Switching the Conductance of Dy Nanocontacts by Magnetostriction. *Nano Lett.* **11,** 574–578 (2011).
13. Jammalamadaka, S. N., Markandeyulu, G., Kannan, E. & Balasubramaniam, K. Development of a magnetostrictive transducer for nondestructive testing of concrete structures. *Appl. Phys. Lett.* **92,** 044102 (2008).
14. Jammalamadaka, S. N., Markandeyulu, G. & Balasubramaniam, K. Magnetostriction and anisotropy compensation in $Tb_xDy_{0.9-x}Nd_{0.1}Fe_{1.93}$ [$0.2 \leq x \leq 0.4$]. *Appl. Phys. Lett.* **97,** 242502 (2010).
15. Zhang, H. Power generation transducer from magnetostrictive materials. *Appl. Phys. Lett.* **98,** 232505 (2011).
16. Clark, A. E. Chapter 7 Magnetostrictive rare earth-Fe2 compounds. In Wohlfarth, E. P. (ed.) *Handbook of Ferromagnetic Materials*, vol. 1, 531–589 (Elsevier, 1980).
17. Cullity, B. D. & Graham, C. D. *Introduction to Magnetic Materials* (Wiley, 2011).
18. Engdahl, G. *Handbook of Giant Magnetostrictive Materials* (Academic Press, 1999).
19. Pei, Y., Fang, D. & Feng, X. Magnetoelasticity of $Tb_{0.3}Dy_{0.7}Fe_{1.95}$ alloys in a multiaxial stress-magnetic field space. *Appl. Phys. Lett.* **90,** 182505 (2007).
20. Jiles, D. C. & Thoelke, J. B. Theoretical modelling of the effects of anisotropy and stress on the magnetization and magnetostriction of $Tb_{0.3}Dy_{0.7}Fe_2$. *J. Magn. Magn. Mater.* **134,** 143–160 (1994).
21. Makk, P. *et al.* Correlation Analysis of Atomic and Single-Molecule Junction Conductance. *ACS Nano* **6,** 3411–3423 (2012).
22. Andrews, D. Q., Cohen, R., Duyne, R. P. V. & Ratner, M. A. Single molecule electron transport junctions: Charging and geometric effects on conductance. *J. Chem. Phys.* **125,** 174718 (2006).

23. Kumar, M. S., Reddy, K. V. & Rama Rao, K. V. S. Effect of Ni substitution on the magnetic and electrical properties of $Dy_{0.73}Tb_{0.27}Fe_2$. *J. Appl. Phys.* **77,** 4589–4594 (1995).
24. Kolesnychenko, O. Y., Shklyarevskii, O. I. & van Kempen, H. Giant Influence of Adsorbed Helium on Field Emission Resonance Measurements. *Phys. Rev. Lett.* **83,** 2242–2245 (1999).
25. Müller, M. *Elektrischer Leitwert von magnetostriktiven Dy Nanokontakten* (KIT Scientific Publishing, Karlsruhe, 2011).
26. Funayama, T., Kobayashi, T., Sakai, I. & Sahashi, M. Mn substitution effect on magnetostriction temperature dependence in $Tb_{0.3}Dy_{0.7}Fe_2$. *Appl. Phys. Lett.* **61,** 114–115 (1992).
27. Clark, A. E., Teter, J. P. & McMasters, O. D. Magnetostriction jumps in twinned $Tb_{0.3}Dy_{0.7}Fe_{1.9}$. *J. Appl. Phys.* **63,** 3910–3912 (1988).

Acknowledgements

S.N.J. would like to thank the Deutscher Akademischer Austauschdienst (DAAD) for financial support through the IIT Faculty Exchange program and the Department of Science and Technology, India, for funding (Project #SR/FTP/PS-190/2012). We acknowledge support by Deutsche Forschungsgemeinschaft and Open Access Publishing Fund of Karlsruhe Institute of Technology.

Author Contributions

S.N.J. and C.S. conceived the experiments, S.N.J., S.K., O.B., W.K. and U.M.K. conducted the experiments, J.A.C. prepared the ingot and performed the XRD measurements, S.N.J. and C.S. analysed the results. All authors reviewed the manuscript.

Additional Information

Competing financial interests: The authors declare no competing financial interests.

How to cite this article: Jammalamadaka, S. N. *et al.* Remote control of magnetostriction-based nanocontacts at room temperature. *Sci. Rep.* **5**, 13621; doi: 10.1038/srep13621 (2015).